XXXVIII International Winter Meeting on Nuclear Physics *LBNL-44840*
24-28 January 2000, Bormio, Italy

Chiral Symmetry Restoration in High-Energy Collisions

Jørgen Randrup*

Nuclear Science Division, Lawrence Berkeley National Laboratory,
University of California, Berkeley, California 94720, USA

High-energy nucleus-nucleus collisions offer the possibility of exploring chiral symmetry in a more global manner than previously. It is expected that the chiral order parameter becomes temporarily very small in the hot collision region and the subsequent non-equilibrium relaxation dynamics may yield isospin-correlated enhancements of soft pions. Dynamical simulations of idealized collision scenarios suggest that this novel phenomenon may be experimentally accessible by suitable event-by-event analyses of the data.

1. INTRODUCTION

Chiral symmetry is believed to be an approximate symmetry of the strong interaction but it is spontaneously broken in the usual low-energy world, with the value of the chiral order parameter in vacuum being $\langle q\bar{q}\rangle = f_\pi \approx 92$ MeV. Therefore, experimental tests of chiral symmetry have been primarily restricted to the broken phase. However, the advent of high-energy nuclear collisions offer an opportunity to perform more global investigations of this fundamental symmetry, since the energy density in the collision zone is expected to exceed the critical value for the restoration of chiral symmetry. If indeed the transient occurrence of such a hot region causes the local order parameter to become significantly reduced in magnitude, then its subsequent non-equilibrium relaxation towards the normal vacuum may generate large-amplitude coherent oscillations of the pion field, commonly referred to as *disoriented chiral condensates.* The key mechanism for this novel phenomenon is illustrated schematically in Fig. 1. The prospects for forming and exploring disoriented chiral condensates has received considerable attention over the past several years (for DCC reviews, see refs. [1–3]).

The most popular theoretical tool for DCC studies has been the linear σ model which describes the O(4) chiral field $\boldsymbol{\phi} = (\sigma, \boldsymbol{\pi})$ by means of a simple effective quartic interaction,

$$\mathcal{L} = \tfrac{1}{2}\partial_\mu \overset{\rightarrow}{\boldsymbol{\phi}} \circ \partial^\mu \overset{\leftarrow}{\boldsymbol{\phi}} - \tfrac{\lambda}{4}(\phi^2 - v^2)^2 + H\sigma \qquad \Rightarrow \qquad [\Box + \lambda(\phi^2 - v^2)] \overset{\leftarrow}{\boldsymbol{\phi}} = H \overset{\leftarrow}{e_\sigma} \ . \tag{1}$$

Invoking this convenient framework, the present discussion reviews the main features of the DCC phenomenon. Moreover, using recent numerical simulations for Bjorken rods as a guide, we identify possible means for extracting experimental DCC signals.

*Work supported by the Director, Office of Energy Research, Office of High Energy and Nuclear Physics, Nuclear Physics Division of the U.S. Department of Energy under Contract No. DE-AC03-76SF00098.

Fig. 1. DCC formation.

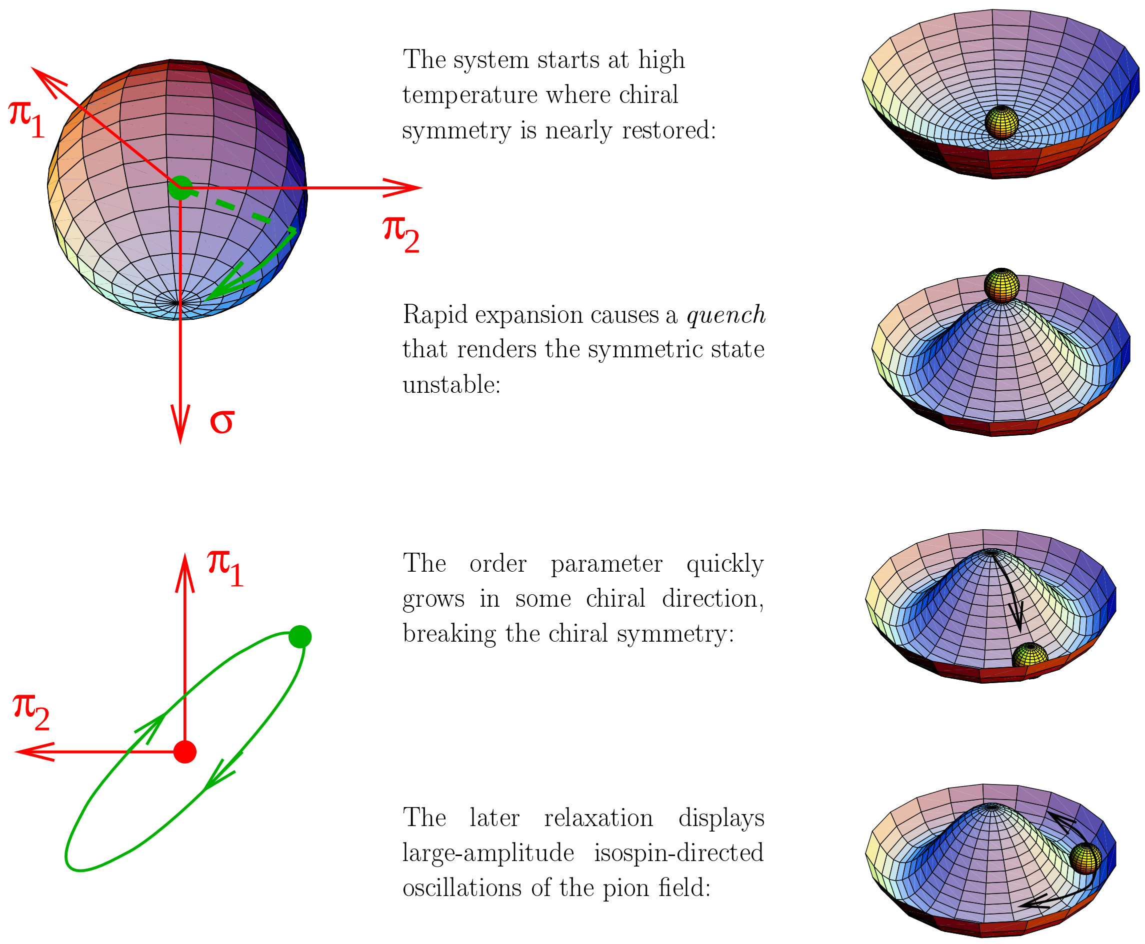

The mechanism leading to DCC formation is illustrated for the simplified worlds in which the isospin space has only two (left-hand side) or one (right-hand side) dimension. In the originally conceived DCC quench scenario, the system is initially so highly agitated that the O(4) order parameter $(\sigma, \boldsymbol{\pi})$ is situated at the single minimum of the effective potential near the origin. The system then expands and/or cools so rapidly that the effective potential quickly reverts to its low-temperature form, in which a nearly degenerate minimum appears as a trough on the surface of the 4-hypersphere with radius f_π, $\sigma^2 + \pi^2 \approx f_\pi^2$. Since the early rapid growth of the order parameter is primarily in the radial direction, the generated vector current $\boldsymbol{\pi} \times \dot{\boldsymbol{\pi}}$ is very small and the subsequent oscillatory relaxation towards the ground state is therefore well directed in isospace (lower left illustration). The emitted pion radiation is then correspondingly isospin polarized, resulting in a very broad distribution of the neutral fraction $f = N_0/(N_- + N_0 + N_+)$.

2. GENERAL FEATURES

In order to gain a feeling for how the chiral degrees of freedom might behave, it is useful to examine the statistical properties of the system. This is best done by considering the partition function associated with the chiral field,

$$\mathcal{Z}_T = \int \mathcal{D}[\boldsymbol{\psi},\boldsymbol{\phi}]\ \exp\left(-\frac{\Omega}{T}E[\boldsymbol{\psi},\boldsymbol{\phi}]\right) = \int d^4\underline{\boldsymbol{\phi}}\ \exp\left(-\frac{\Omega}{T}F_T(\phi_0,\chi_0)\right)\ . \tag{2}$$

Here the functional integral is over all possible fields $\boldsymbol{\phi}(\mathbf{r})$ and their time derivatives $\boldsymbol{\psi}(\mathbf{r})$. The statistical weight for finding the system with a specified value of the order parameter $\underline{\boldsymbol{\phi}}$ is given in terms of the associated free energy density which depends only on the magnitude of the order parameter, ϕ_0, and the angle of disorientation, χ_0 (with $\underline{\sigma} = \phi_0 \cos\chi_0$). The order parameter $\underline{\boldsymbol{\phi}}$ can be thought of as representing the smooth local average of the field which generally varies rapidly in space. The residual components then represent quasi-particle excitations relative to the constant background characterized by the order parameter; these quasi-particles are endowed with effective masses that depend on the medium through both the local order parameter and the local field fluctuations. For more details, see Refs. [4,5].

Fig. 2. Free energy.

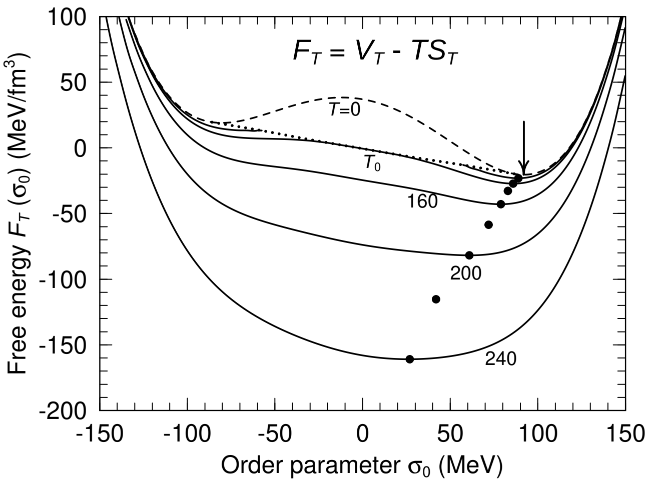

The free energy density F_T along the σ axis, for a range of temperatures T (solid curves). (The starting points for $T<T_0$ are connected by the dotted curve, while the dashed curve shows the result obtained when the temperature is neglected.) The arrow points to the minimum of $F_{T=0}$ and the solid dots indicate the location of the minima for finite temperatures. [4]

The above expression (2) makes it possible not only to determine the thermodynamically preferred value of the order parameter (namely that value of ϕ_0 which yields the minimum value of the free energy, as illustrated in Fig. 2 above), but also to calculate the entire statistical distribution of the order parameter in finite systems (as illustrated in Fig. 3). It should be noticed that the distribution of the order parameter is fairly well-confined and its transverse magnitude never grows very large. Thus, the degree of disorientation is fairly modest, even at high temperatures (for realistic values of the parameter H which governs the O(4) symmetry breaking.) Consequently, even when heated well above the critical temperature, the chiral order parameter retains a clear preference for an orientation towards the positive σ direction, a result somewhat different from the idealized picture presented in Fig. 1.

Fig. 3. Distribution of the order parameter.

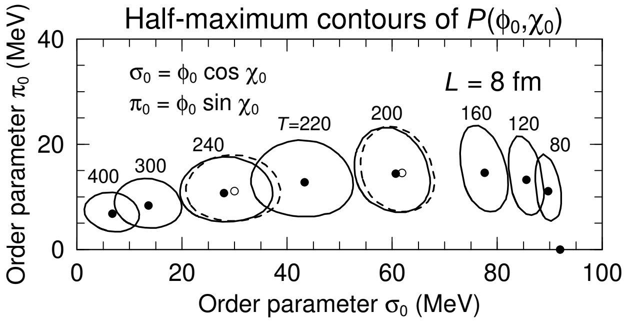

Projection of the probability $P(\underline{\phi})$ onto ϕ_0 (the magnitude of the order parameter) and χ_0 (the disalignment angle) is displayed as a function of $\sigma_0 = \phi_0 \cos \chi_0$ and $\pi_0 = \phi_0 \sin \chi_0$, for a cubic box of side length L=8 fm. Solid contours: scaled continuum results; dashed contours: quantized quasi-particle modes. [4]

While the thermal properties provide useful insight, they are of limited utility for understanding the non-equilibrium evolution of the chiral degrees of freedom. It is therefore helpful to replace the temperature by the average field fluctuation, $\Delta\phi = \langle \delta\boldsymbol{\phi} \circ \delta\boldsymbol{\phi} \rangle^{1/2}$, since this quantity is meaningful for any individual field configuration $\boldsymbol{\phi}(\mathbf{r})$. The resulting display provides a useful "Road Map" for chiral dynamics (Fig. 4).

The early violent part of the collision injects the system into the upper-left portion of the diagram (where the agitation is large and the order parameter correspondingly small) and it will then develop towards the vacuum situated near the lower-right corner of the display. Generally, the fast expansion will promptly pull the system out of equilibrium.

Fig. 4. Chiral Road Map.

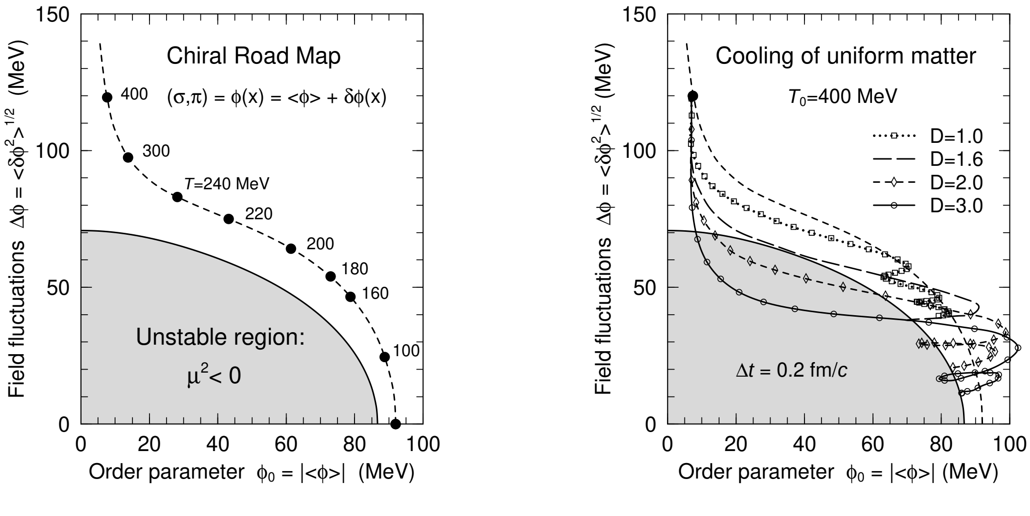

Left panel: The equilibrium path on the *Chiral Road Map* in which the field configuration is projected onto a single point, $\boldsymbol{\phi}(\mathbf{r}) \rightarrow (\phi_0, \Delta\phi)$. The adiabatic path of equilibrium points (dashed curve), which represents the major "highway", exhibits a gradual cross over from the broken phase at low temperature to the nearly restored phase at high temperature. The shaded area covers the classically forbidden region within which the effective field is supercritical.
Right panel: The dynamical paths of systems that have been prepared in equilibrium at T_0 = 400 MeV and then subjected to a Rayleigh cooling with strengths D adjusted to emulate scaling expansions (D=1 emulates a longitudinal Bjorken expansion). [6]

In actual collision scenarios, the expansion is likely to be primarily longitudinal, at least initially, with some transverse expansion gradually appearing in response to the high interior pressure generated. It appears that a pure longitudinal expansion (D=1) is insufficient to bring the system into the supercritical region, as the dynamical trajectory never strays far from the adiabatic path. On the other hand, an isotropic scaling expansion (D=3) would produce a quench-like scenario by forcing the system well into the unstable region where spontaneous pion pair creation is possible. (The resulting scenario of rapid amplification of soft modes is qualitatively similar to the idealized quench [7].) Thus it is a rather delicate question whether the dynamics will lead to supercriticality.

On the other hand, a much more robust feature is the eventual oscillation of the order parameter as it relaxes towards its vacuum value. As is evident from Fig. 4 (right panel), the entire range of cooling rates lead to such a behavior (although the amplitude is larger for the more rapid scenarios). This characteristic time dependence of the order parameter is reflected in the effective pion mass and, consequently, one may expect significant enhancements of the pion yield (and the associated photon [8,9] and dilepton [10] yields) in the affected parts of phase space. Figure 5 illustrates how a pure harmonic perturbation would act. In reality, the amplitude of the oscillation subsides in time and this introduces a bias in favor of the soft modes (see Fig. 8).

Fig. 5. Effect of harmonic perturbation.

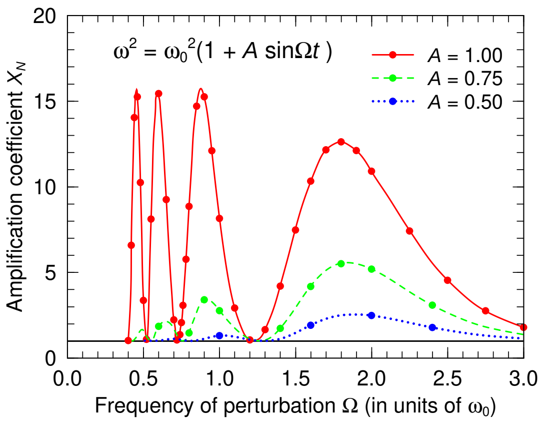

A free particle is subjected to a harmonic perturbation of its mass, so that its frequency is of the form $\omega^2(t) = \omega_0^2[1 + A\sin\Omega t]$. The equation of motion then has the Mathieu form, resulting in a resonant behavior as a function of the perturbation frequency Ω. Thus, the number of quanta in mode is enhanced, $N(t) = X_N(t)[N(0)+\frac{1}{2}]-\frac{1}{2}$. The enhancement coefficient $X_N(t)$ is shown after two periods of perturbation, as a function of the perturbation frequency Ω (in units of ω_0) and for three values of the amplitude A. [11]

3. BJORKEN ROD SIMULATIONS

Although the idealized scenarios briefly discussed above can yield very instructive insight into key features of the DCC phenomenon, it is important to consider more realistic scenarios in order to ascertain the prospect for extracting signals in actual experiments. For this purpose it is interesting to consider the evolution of a cylinder subjected to a longitudinal scaling expansion of the Bjorken type. This scenario (already considered in Ref. [12]) contains some of the important features expected in real collision events, in particular, [1]) it has a surface region through which the order parameter changes from its value in the bulk of the interior to its vacuum value outside and [2]) it is in a state of rapid expansion. The features of the initial field configuration are illustrated in Fig. 6.

Fig. 6. Initial transverse profiles of the Bjorken rod.

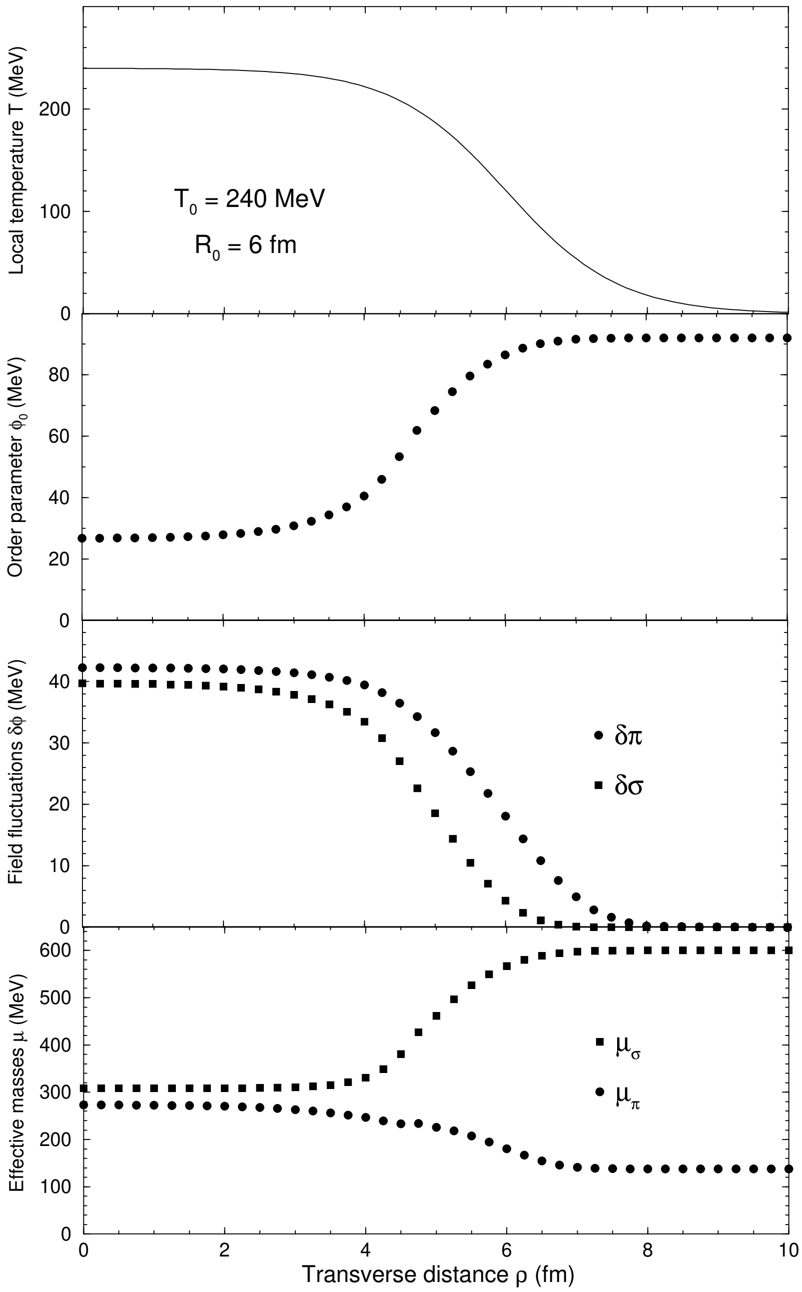

The transverse temperature profile (taken to be of Saxon-Woods form) as given in terms of the specified local temperature $T(\rho)$, for a cylindrical rod with a radius of $R_0 = 6$ fm and a central temperature of $T_0 = 240$ MeV.

The corresponding distance dependence of the order parameter ϕ_0, which increases from its small central value of around 28 MeV (which is given by the equilibrium value at $T{=}T_0$) towards its value in the vacuum, $f_\pi = 92$ MeV.

The magnitude of the initial local fluctuation of the chiral in a given O(4) direction, for either the σ component, $\delta\sigma$, or one of the three equivalent pion components, $\delta\pi$.

The effective masses μ_σ and μ_π as functions of ρ. In the bulk region, where the order parameter is small, the effective masses are nearly degenerate, but they diverge in the surface region and approach their vacuum values outside.

The initial state represents a diffuse cylindrical rod endowed with an inherent longitudinal expansion of the Bjorken scaling type and the above plots illustrate how the local environment changes in the transverse direction (for details, see Ref. [13]). The rod interior corresponds to bulk matter at the temperature T_0. The individual field components change smoothly through the surface region and approach their appropriate constant vacuum values outside. The specified values T_0 and R_0 characterize an entire ensemble of microscopically different field configurations and a corresponding statistical sampling is made so that the dynamical simulations are carried out for a suitably large sample of individual systems.

Once the initial state has been specified, it is propagated numerically by means of the field equation (1), until sufficiently late times when effective decoupling has occurred and the system consists of freely moving particles. (Generally it is hard to treat fields in expanding scenarios, but the idealized nature of the Bjorken expansion makes the problem tractable by transforming from t, z to τ, η, with $t = \tau \cosh \eta$ and $z = \tau \sinh \eta$.)

The dynamical development of the rod interior is plotted on the *Road Map* in Fig. 7, together with the development of Bjorken matter prepared with the same initial temperature T_0. (Bjorken matter is bulk matter subjected to a Bjorken expansion in one direction and thus represents approximately the condition inside the rod early on before the transverse expansion of the rod has become significant.) It is seen that the development resembles the results shown in Fig. 4 (right panel) for the case of $D = 1$, the cooling rate emulating the longitudinal expansion. Furthermore, at early times, the development in the rod interior is indeed very similar to that of the corresponding Bjorken matter. However, since the transverse expansion of the rod leads to a larger rate of cooling, the relaxation towards the vacuum conditions proceeds more rapidly for the rod and, consequently, the effect of the order parameter oscillations is reduced (see Sect. 3.1).

Fig. 7. Phase evolution of the rod.

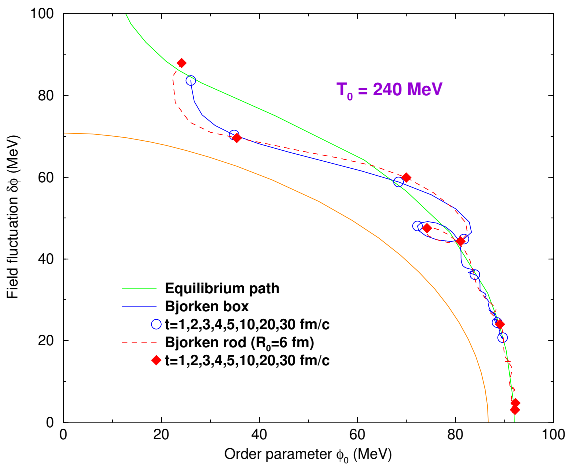

The phase evolution of the interior of the Bjorken rod compared with the corresponding evolution of Bjorken matter. The information for the rod has been obtained by averaging over a hollow cylindrical volume, $1<\rho<3$ (fm). The symbols indicate the location of the paths at successive proper times $\tau = 1, 2, 3, 4, 5, 10, 20, 30$ fm/c. The two evolutions are similar early on, but then the rod relaxes significantly faster due to the generated transverse expansion. [13]

In the Bjorken expansion scenario, the analysis of the resulting asymptotic state is most conveniently done by Fourier transforming the pion field over the transverse xy plane. This procedure yields the quantities $\{\bar{n}_{\mathbf{k}}^{(j)}(\mathrm{y}_1, \mathrm{y}_2)\}$ which represent the expected number of pions of a given charge state j $(+, -, 0)$, moving with the transverse momentum $\mathbf{k}$, and having a rapidity in the interval $(\mathrm{y}_1, \mathrm{y}_2)$. (Usually we consider unit rapidity intervals and may refer to each of these as a rapidity "lump".)

It should be noted that the quantities $\bar{n}$ represent the properties of the *field* and may be interpreted as the *expected* multiplicity. The *actual* multiplicity is a stochastic variable which in general depends on the quantum correlations present. For uncorrelated many-body states, the multiplicity is a Poisson distribution, but the non-equilibrium time evolution introduces significant correlations requiring a real-time quantum field treatment.

3.1. Transverse spectra

The simplest quantity to extract is the transverse spectrum, $Ed^3N/d^3\mathbf{p} = d^3N/d^2\mathbf{k}dy$. The transverse spectral shape is well approximated by an equilibrium form above kinetic energies of 200 MeV or so, while a clear excess yield is present at lower energies. The resulting ratio between the dynamical spectrum and the corresponding Bose-Einstein form is displayed in Fig. 8 for $T_0 = 240$ MeV, together with the corresponding matter result. While the quality of the fit for rods is as good as for matter, the ensuing soft enhancements are generally smaller. This is not surprising, since the bulk conditions prevail in only part of the rod configuration and, moreover, the transverse expansion tends to suppress the oscillatory relaxation causing the enhancement. Figure 9 shows the dependence of the pion excess on the initial temperature and rod radius.

Fig. 8. Spectral shape for Bjorken rods.

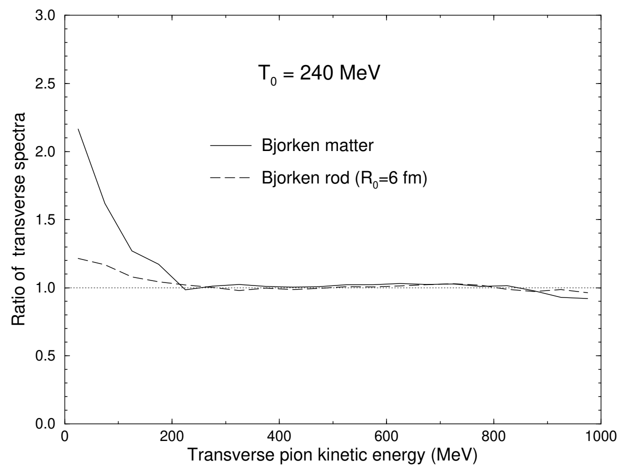

The ratio between the final transverse pion spectrum, $d^3N/d^2\mathbf{p}_\perp dy$, and the associated equilibrium spectrum obtained by fitting the dynamical result with a Bose-Einstein form within the energy interval 200-1000 MeV, for a longitudinally expanding rod (dashed curve) having an initial radius of $R_0 = 6$ fm and with an initial bulk temperature of $T_0 = 240$ MeV, as well as the result for the corresponding Bjorken matter. [13]

Fig. 9. Excess of soft pions for Bjorken rods.

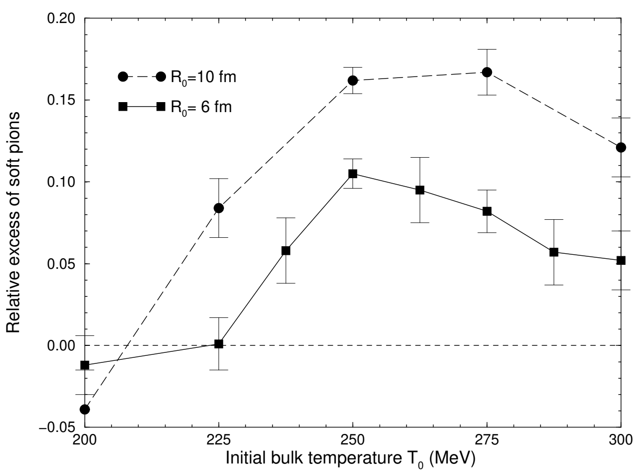

The relative excess of pions for Bjorken rods with initial radii R_0 equal to either 6 or 10 fm, as a function of the initial bulk temperature T_0. The excess has been obtained by subtracting the yield of pions with kinetic energies below 200 MeV from the corresponding equilibrium spectrum obtained by fitting the dynamical result with a Bose-Einstein form within 200-1000 MeV. Realistic rod radii are probably significantly larger and so the present result may provide lower bounds. [13]

Since the excess pions reflected in the spectral enhancement are produced by the coherent oscillation of the order parameter, their properties are expected to differ from the regular pions. Therefore, in order to better bring this out, it is useful to consider the soft and hard pions separately in the following analyses.

3.2. Multiplicity distributions

In order to investigate whether the resulting multiplicity distributions contain deviations from the relatively trivial Poisson statistics, we have extracted the associated factorial moments. Because of the enhancement of the soft pions seen in the transverse spectra, we consider the pions below and above 200 MeV separately. For multi-particle final states, one may define the following factorial moments,

$$\mathcal{M}_m \equiv \prec N(N-1)\cdots(N-m+1) \succ \quad . \tag{3}$$

Here N is the number of pions emitted by a given rapidity lump of unit length and the average is over all lumps in a sample of events prepared in the same manner (*i.e.* same bulk temperature T_0 and rod radius R_0). The contribution to $\mathcal{M}_m$ vanishes for a lump with a multiplicity smaller than the particular order m. For a Poisson multiplicity distribution characterized by the mean multiplicity $\bar{N} = \mathcal{M}_1$, the factorial moments are simply given by $\mathcal{M}_m = \mathcal{M}_1^m$. It is therefore preferable to consider the reduced factorial moments, $\mathcal{M}_m/\mathcal{M}_1^m$, which are then all unity for a Poisson multiplicity distribution. Since $\bar{N}$ is not available experimentally, the average of the observed multiplicities for each lump has been used instead, $\prec N \succ$, presumably a good approximation since the lumps are all macroscopically equivalent.

Figure 10 shows the relative factorial moments obtained for a sample of Bjorken rods prepared with $T_0 = 250$ MeV and $R_0 = 6$ fm. (We consider from now on systems prepared with $T_0 = 250$ MeV, since the soft enhancement is largest near this temperature.) While the hard pions appear to be perfectly consistent with pure Poisson statistics, the soft pions exhibit a significant non-poissonian behavior. The character of the deviation of the soft factorial moments suggests that the source occasionally emits anomalously many pions, as one would expect if some modes are preferentially amplified. This feature is consistent with the enhancement of the soft spectrum and it can also be explored by other means of analyzing the data for anomalous fluctuations.

Fig. 10. Reduced factorial moments.

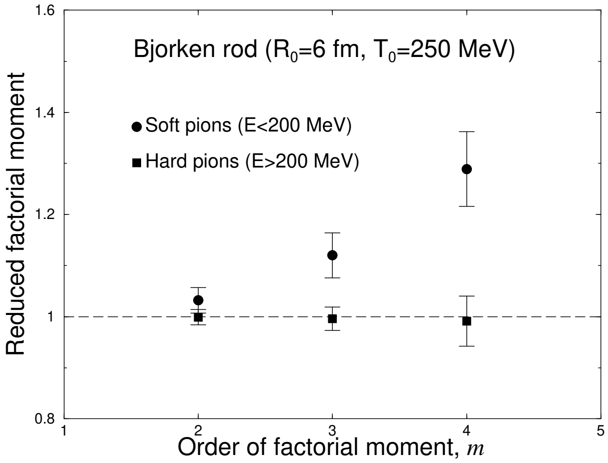

The reduced factorial moments $\mathcal{M}_m/\mathcal{M}_1^m$ obtained for a sample of rods prepared with $R_0 = 6$ fm and $T_0 = 250$ MeV and displayed as functions of the order m, for either soft (dots) or hard (squares) pions emitted within a given rapidity interval of unit length (a "lump"). The error bars arise from the sampling over all lumps and events. The reduced factorial moments for a pure Poisson multiplicity distribution are all unity. [13]

3.3. Azimuthal emission patterns

When averaged over events, the emission probability has overall cylindrical symmetry, due to the symmetry of the initial ensemble of fields. Similarly, due to the boost invariance of the ensemble, the averaged emission probability is independent of the rapidity. And, thirdly, the isospin invariance of the ensemble guarantees that all three types of pion behave similarly after the event average has been carried out. Though each individual lump retains these symmetries in a macroscopic sense, texture exists at the microscopic level. This important feature is manifested as fluctuations in the underlying expected differential mean multiplicities $\bar{n}^{(j)}_{\mathbf{k}}(\mathsf{y}_1,\mathsf{y}_2)$, from one rapidity interval to the next and from event to event.

The fluctuations in the azimuthal emission pattern can be elucidated by means of the following multipole moments,

$$\tilde{\alpha}^{(j)}_{M}(\mathsf{y}_1,\mathsf{y}_2) \;\equiv\; \frac{1}{E_\perp}|\sum_{\mathbf{k}} \bar{n}^{(j)}_{\mathbf{k}}(\mathsf{y}_1,\mathsf{y}_2) E_k\ \mathrm{e}^{iM\phi_{\mathbf{k}}}|\ . \tag{4}$$

The weighting by the transverse kinetic energy $E_k \equiv m_k - m_\pi$ ensures that particles emitted with very low transverse momentum have little effect, as is reasonable since their particular azimuthal direction is physically insignificant. Because of the spectral enhancement of the soft pions discussed above, it is useful to extract the multipole strength distribution for soft and hard pions separately. Finally, $E_\perp \equiv \sum_{\mathbf{k}} \bar{n}_{\mathbf{k}} E_k$ denotes the total mean transverse kinetic energy of the soft or hard pions emitted by a given rapidity lump. (The second-order multipole coefficient gives a rough indication of the quadrupole moment and is related to the coefficient v_2 introduced in Ref. [14] for elliptic flow.)

In each individual event, and for each of the three pion types separately, the multipole moments are calculated for the pions arising from each separate rapidity lump. Because of the independence of different events, the isospin symmetry, and the longitudinal boost invariance, respectively, all the individual lumps present equivalent sources and hence we may perform a subsequent average, yielding $\prec \tilde{\alpha}_M \succ$.

The resulting ensemble average azimuthal multipole strength function is displayed in Fig. 11. for the soft and hard modes of the asymptotic pion field. Two different Bjorken rod scenarios are displayed, both having the initial bulk temperature is $T_0 = 250$ MeV, but the initial radius R_0 being either 6 fm or 10 fm. In order to get an idea of the significance of the extracted values, we have calculated an auxiliary set of moments, $\tilde{\alpha}^{\mathrm{random}}_{M}$, obtained by turning each individual emission direction $\phi_{\mathbf{k}}$ by a random angle before evaluating the multipole moment.

The azimuthal coefficients for soft pions, considered as a function of the multipolarity M, start out well above the noise level, then exhibit a gradual drop-off. For high multipolarities, the moments approach zero because the high-frequency components of the field are suppressed by the initial thermal weight.

The corresponding multipole coefficients extracted for the hard pions are initially an order of magnitude smaller than those for the soft pions but they exhibit a significantly gentler fall-off with the multipolarity M, suggesting a correspondingly narrower angular correlation. This is consistent with the general expectation that harder pions exhibit a smaller spatial correlation length. As for the soft modes, the wider rod yields smaller multipole coefficients.

Fig. 11. Multipole strength of soft and hard pion modes.

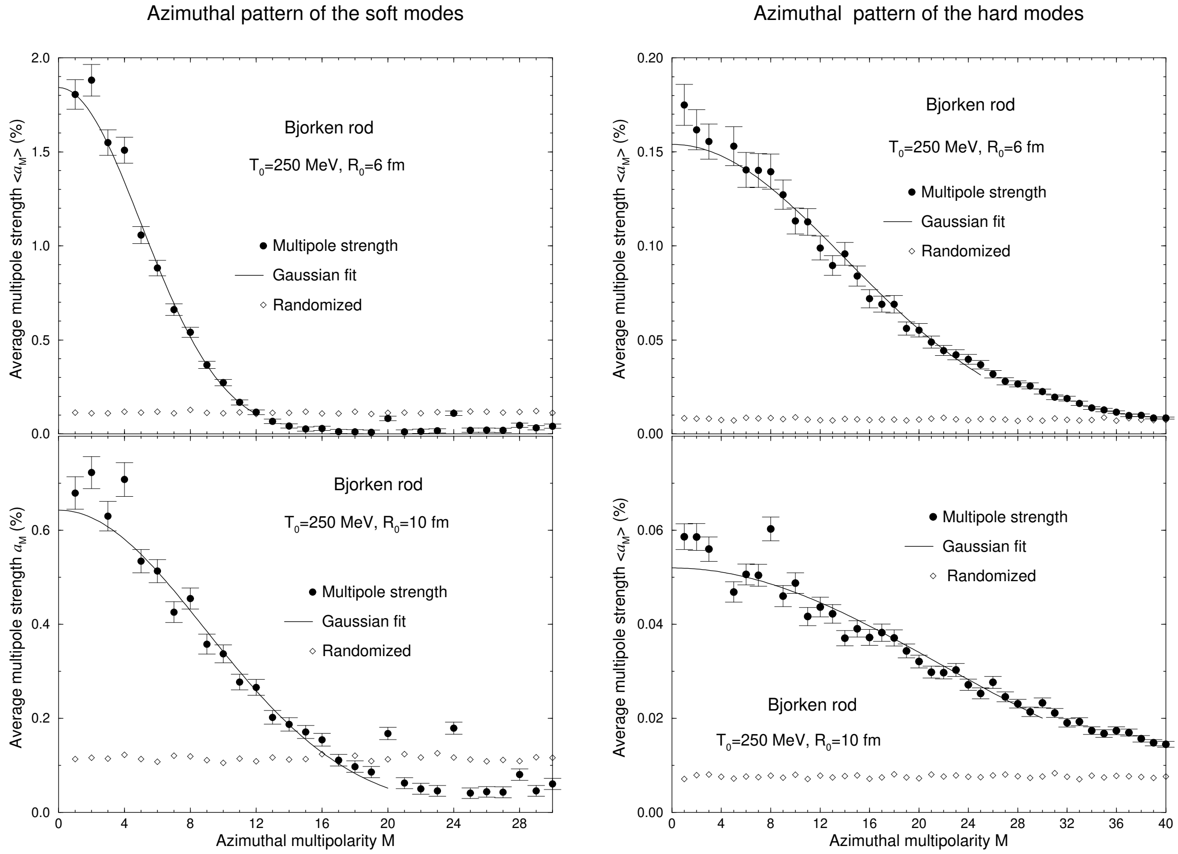

The azimuthal multipole strength distribution (in per cent) for the soft (left) and hard (right) modes of the asymptotic pion field, $\tilde{\alpha}$ (solid circles), extracted for an ensemble of events starting with an initial rod radius R_0 of either 6 or 10 fm and an initial bulk temperature of $T_0 = 250$ MeV. The solid curve shows the gaussian fits. The open diamonds indicate the noise level obtained by randomizing the azimuthal directions $\phi_{\mathbf{k}}$ before evaluating the multipole moment. [13]

The behavior of the multipole strength provides information on the domain structure of the source. The attenuation of the strength with increasing multipolarity M can be reasonably approximated by a gaussian fit which makes it possible to extract the dispersion of the curve, ΔM. The usual inverse relationship between conjugate variables, then yields the azimuthal correlation length, $\Delta\phi = 1/\Delta M$. Thus, if the effective transverse size of the source is R, the spatial domain size is given by $\approx R\Delta\phi$. For the two scenarios having the initial rod radius R_0 equal to 6 and 10 fm, we extract ΔM as 5.03 and 8.84, leading to values of $\Delta\phi$ equal to $11.^{\circ}4$ and $6.^{\circ}5$, respectively. Since $R_0\Delta\phi$ is thus approximately the same in the two scenarios, the spatial correlation length at the effective emission time appears to be independent of the initial radius of the rod. This is as one would expect if that quantity reflects the conditions in the source at the time of effective decoupling.

It should be emphasized that although the above analysis is based on the *field*, a corresponding analysis of the resulting *particles* (using a simple Poisson sampling) yield largely identical results [13], thus allowing a practical analysis.

3.4. Neutral pion fraction

The distribution of the neutral pion fraction $f \equiv N_{\pi^0}/N_{\rm tot}$ has received considerable attention as a DCC diagnostic because an idealized fully isospin-polarized source (a "domain") would yield an anomalously wide distribution, $P_0(f) = 1/2\sqrt{f}$, rather than a narrow peak around the average value $f = \frac{1}{3}$. Indeed, experiments have been devoted to the search for anomalous behavior of the neutral pion fraction [15,16]. However, such an undertaking is quite difficult, partly because the signal is expected to be carried by only the soft pions and partly because the extraction of f requires the simultaneous event-by-event measurement of both charged and neutral pions.

Furthermore, it is important to adjust the scope of the analysis so as to optimize the signal: If the employed acceptance is too large then several domains are sampled and the combined isospin polarization is then diminished, while too small an acceptance degrades the statistics. This inherent feature is illustrated below where Fig. 8 shows the effect of combining independent sources and Fig. 9 illustrates how the signal can be enhanced by considering azimuthal sections in the analysis of the dynamical rod results. Generally, the soft pions give rise to a wider distribution than the hard pions.

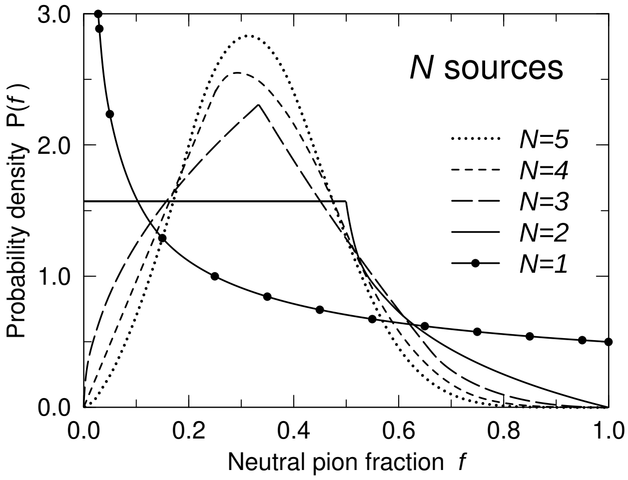

Figure 12. The distribution of the neutral fraction f resulting from N similar sources having independent isospin alignments. As N is increased, $P(F)$ evolves from a very broad distribution towards a narrow peak around $f = \frac{1}{3}$ and the associated variance is given by $\sigma_f^2 = 4/45N$ (which is still larger than a corresponding unpolarized emission would give). [5]

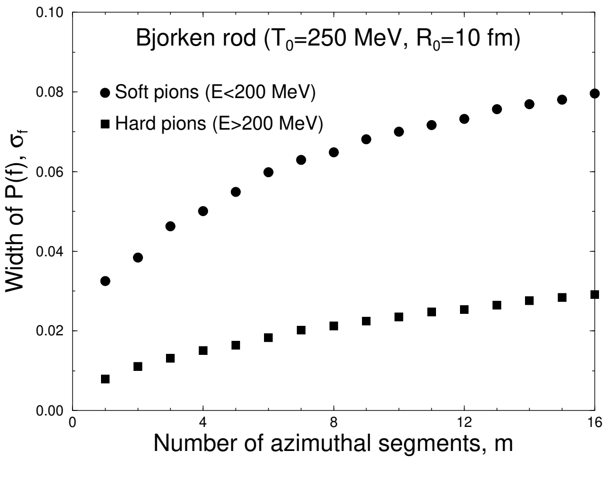

Figure 13. The dispersion σ_f of the neutral pion fraction distribution $P(f)$ for sources that have been obtained by dividing each rapidity lump into m equally large azimuthal sections of width $2\pi/m$, based on an ensemble of rods with a initial bulk temperature $T_0 = 250$ MeV and radius $R_0 = 10$ fm. Results for both soft and hard pions are shown. [13]

4. CONCLUSION

The present discussion has focussed the prospects for achieving experimental information on the effect of the approximate chiral symmetry restoration expected to occur in high-energy nuclear collisions.

Because of the complexity of the problem, and our relative ignorance about a number of the key elements, it is hard to make reliable theoretical predictions about these phenomena. For example, only effective theories are practically tractable, and even at that relatively simple level a full non-equilibrium real-time quantum-field treatment is presently beyond practicality. Moreover, the extension of the model to SU(3) in order to include strangeness has been found to have significant effects [17] but this has not yet been incorporated. Finally, a more realistic scenario would contain other degrees of freedom as well, including a hadronic halo, but such hybrid descriptions are not well established.

Because of such approximations and idealizations, the theoretical results serve merely to elucidate the importance of some of the complications that are inevitably present in any real system produced by high-energy collisions (*e.g.* surface and expansion). Generally speaking, the results suggest that while one should not expect spectacular DCC signals in the actual data, carefully designed quantitative analyses might bring out any anomalous DCC-type behavior in the data. In particular, the consideration of the transverse spectrum, the factorial moments, and the multipole strength may be illuminating.

REFERENCES

1. K. Rajagopal, in *Quark-Gluon Plasma 2*, ed. R. Hwa, World Scientific (1995)
2. J.-P. Blaizot and A. Krzywicki, Acta Phys. Polon. B27 (1996) 1687
3. J.D. Bjorken, Acta Phys. Polon. B28 (1997) 2773
4. J. Randrup, Phys. Rev. D55 (1997) 1188
5. J. Randrup, Nucl. Phys. A616 (1997) 531
6. J. Randrup, Phys. Rev. Lett. 77 (1996) 1226
7. K. Rajagopal and F. Wilczek, Nucl. Phys. B404 (1993) 577
8. Z. Huang and X.N. Wang, Phys. Lett. B383 (1996) 457
9. D. Boyanovsky, H.J. de Vega, R. Holman, and S. Prem Kumar, PRD56 (1997) 5233
10. Y. Kluger, V. Koch, J. Randrup, and X.N. Wang, Phys. Rev. C57 (1998) 280
11. J. Randrup, Heavy Ion Phys. 9 (1999) 289
12. M. Asakawa, Z. Huang, and X.N. Wang, Phys. Rev. Lett. 74 (1995) 3126
13. T.C. Petersen and J. Randrup, Phys. Rev. C61 (2000) 024906
14. A.M. Poskanzer and S.A. Voloshin, Phys. Rev. C58 (1998) 1671
15. MiniMax Collaboration (T.C. Brooks *et al.*.), Phys. Rev. D55 (1997) 5667
16. WA98 Collaboration (M.M. Aggerwal *et al.*.), Phys. Lett. B420 (1998) 169
17. J. Schaffner-Bielich and J. Randrup, Phys. Rev. C59 (1999) 3329